Accelerated Heat Transfer Simulations Using Coupled CFD and DEM

Marina Sousani*, Andrew M. Hobbs[1], Adam Anderson[2], Richard Wood*

* DEM Solutions LTD, 49 Queen Street, Edinburgh, EH2 3NH
e-mail: marina.sousani@edemsimulation.com, web page: http://www.edemsimulation.com/

[1]Astec, Inc.
4101 Jerome Ave. Chattanooga, Tennessee, 37407, USA
e-mail: ahobbs@astecinc.com, web page: http://www.astecinc.com

[2]ANSYS UK Ltd.
Sheffield Business Park, 6 Europa View, Sheffield, S9 1XH, UK
e-mail: adam.anderson@ansys.com

Abstract

This work presents an accelerated simulation of heat and mass transfer by coupling Discrete Element Methodologies (DEMs) and Computational Fluid Dynamics (CFD), utilising Graphics Processing Unit (GPU) technology. The presented model is a continuation of previous work[1] and focuses on demonstrating the capabilities and effectiveness of implementing the GPU combined with the Central Processing Unit (CPUs) technologies to run a complex industrial simulation. A model of an aggregate drum dryer was used to produce hot mix asphalt and different configurations have been implemented to investigate the effect of GPU-CPU technology in such a complex simulation. Commercial codes from ANSYS and DEM-Solutions were coupled to simulate heat transfer from the hot gases to the aggregate particles. Fluid flow and particle-fluid interactions are solved by the CFD solver which exchanges information at regular intervals. The results showed that the coupled model captures accurately the convective heat transfer from the fluid to the solid phase and demonstrated significant improvement in terms of simulation time. The proposed model will have a significant impact in industrial applications as it describes a methodology to simulate large-scale applications rapidly and accurately.

Keywords: coupled DEM and CFD; GPU; aggregate dryer; heat and mass transfer

Introduction

Particle simulations have been well established as a means to model complex physical systems in a number of fields and are becoming increasingly more important in others. Much research has been done in a variety of areas such as molecular dynamics, plasma physics, fluid dynamics and rock mechanics [2-4], where particle simulations were coupled with Computational Fluid Dynamics (CFD)[5]. The Oil and Gas industries have been using CFD software for many years to model fluid behaviour in reservoirs, saturation of residual oil, well performance, fluidisation, sedimentation and others [6-11]. Lately the ability to simulate larger number of particles, especially for applications where particle-particle interaction and particles of different shape must be considered, has given a boost to the demand for more coupled DEM-CFD simulations.

Recently this type of modelling shows an increasing interest in the process manufacturing industry too. Hot mix asphalt (HMA) is the most common pavement surface in the U.S., which comprises around 94% of all roads. It is also increasingly popular in airport runways in the U.S. due to its efficiency on takeoffs and landings, its low maintenance and fast construction time. It has been approved by the

Environmental Protection Agency (EPA) and is thus considered a practical solution for water storage, flood control, erosion and hazardous-waste landfills worldwide [12-14]. HMA is a composite material that consists of mineral aggregates (sand and various sizes of crushed rock) mixed together with liquid asphalt cement binder (a product of crude oil), laid in layers and compacted. For an efficient mixing process, the asphalt binder must be heated at temperatures above 180ºC, to decrease its viscosity, and the aggregate must be dried prior to mixing [13]. Most aggregate is stored in stockpiles where the minimum moisture content will be that of the ambient air. A typical value for aggregate moisture content is 5% by mass meaning that for a nominal production rate of 320,000 kg/h of mix, 15,875 kg/h of H_2O must be removed. Typically, half of the total heat input is required to dry the aggregate making drying efficiency of critical importance [1].

The aggregate drying process is accomplished in a counter flow drum that is positioned on a 4.7º inclination and contains internal metal slats (flights). The drum is heated by a direct fire burner and the flights lift and veil the aggregate material through the hot gases to heat and dry the aggregate particles. Wet aggregate is fed into the uphill end and is moved along the drum towards the burner (Figure 1).

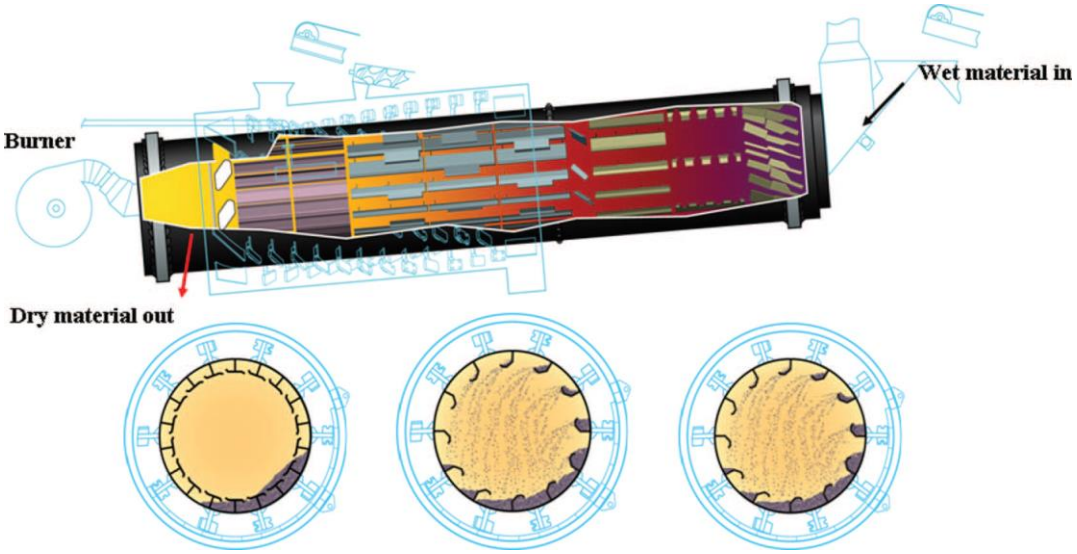

Figure 1 *Schematic of the Counter-flow aggregate dryer drum. Hobbs (2009).*

A key challenge associated with this process is the fact that veiling performance is tied to many different variables including flight shape, number of flights, drum rotational speed, and fill level. At the same time, direct observation of this phenomenon is impossible due to the harsh internal environment of the drum. Part of the aim of this work is to propose a methodology that enables not only the monitoring of the material's behaviour but the optimization of the flight design for increased drying efficiency. Furthermore, this paper presents an innovative way of accelerating such demanding simulations by performing DEM calculations in GPU mode while solving for the fluid in CPU mode.

Numerical methods

CFD is a very popular method amongst researchers that simulates fluid phenomena and provides qualitative prediction of fluid flows. A first appearance of CFD methods dates back to 1947 from the work of Kopal (1947) of supersonic flows on sharp cones and the first generation of CFD solutions the period between the 1950s and early 1960s [16-19]. Since then, the role of CFD in engineering predictions has been so strong that nowadays is considered a standard aspect in fluid dynamics, beyond the experimental and theoretical elements. A wide range of industrial applications employ CFD methods to study critical fluid phenomena and enhance their operations [1, 20-23]. There are commercial

software that have been used for modelling multiphase, combustion and heat transfer for particle flows including densely packed systems such as fluidized bed reactors. However, in some applications it is critical to account for the shape and the particle-particle interactions of the granular material, to provide a meaningful insight.

DEM is a method that describes the overall (macroscopic) mechanical behaviour of assemblies of particle systems as the result of the interaction of their constitutive individual elements. It allows displacements, rotations and complete separation of the discrete elements, and recognizes any new contacts that are developed during the simulation [24, 25]. Initially models, which were based on the particle-scale, were developed in order to simulate the micromechanical behaviour of soils and sands (non-cohesive materials) [26], but since then it has been widely utilised in a number of studies. DEM has been applied in several engineering fields, such as slope stability and mining to powder technology, minerals and process manufacturing [3, 4, 27-32], and is considered a very efficient engineering tool.

In nature particles rarely operate within systems that are fluid free, hence there is a need for a simulation methodology that can capture both the solid and the fluid mechanisms as well as the interaction between the two. Researchers have worked towards combining CFD techniques with the Newtonian particle methods used in DEM. Approaches that incorporate CFD with the DEM have been presented by Tsuji (1993), Tsuji (2008) and Xu and Yu (1997), where the interaction between the solid and gas phases have been modelled by solving Newton's second law of motion, with respect to the motion of the particles, and the Navier-Stokes equation with respect to the motion of the gas. However, the majority of the CFD-DEM approaches involve in-house codes making them inaccessible and expensive to industry. This paper presents an improved version of an existing commercial product that couples the CFD solver (ANSYS Fluent) with the DEM solver (EDEM) from DEM Solutions. The EDEM-CFD coupling is employed to simulate heat transfer from a reacting natural gas flame to the particle phase in an aggregate dryer.

Moreover, complex industrial applications that involve hundreds of thousands of particles are so computationally expensive that not even the most efficient couplings are able to support. This paper presents an innovative way of accelerating computationally intensive workloads by performing DEM calculations in GPU mode while solving for the fluid in CPU mode. The presented solver provides greatly reduced computational times compared to simulations on multi-core CPUs. This process has been performed with the use of the EDEM GPU solver engine, which has been created by DEM Solutions.

DEM – CFD Coupling Methodology

CFD

In previous work [1] particle positions and interactions were solved by the DEM solver, whereas the volume fraction, drag, and heat transfer were calculated by the coupling interface between the solvers. This required significant computation outside of the solvers making this approach less efficient for simulations that required large number of particles. Advantage has now been taken of developments in Fluent since the previous coupling and the latest Fluent solver presents a more sophisticated approach. Specifically, in the new Dense Discrete Phase Model (DDPM) coupling the EDEM particle data are converted into a Discrete Phase Model (DPM) injection and the volume fraction, drag, and heat transfer are calculated directly by Fluent, making for a more efficient calculation.

The volume fraction (the space occupied by each phase), in any given fluid cell, is calculated through an algorithm that utilises an octree method and detects those cells containing particles during the simulation. The flow of the fluid, around the particles, is then determined by the continuous phase flow while taken into account the blockage from the solid phase. Here, the volume fraction represents the space occupied by each phase, thus the laws of conservation of mass and momentum are satisfied by

each phase individually. The mass and momentum conservation equations for the particle phase p are given by:

$$\frac{\partial}{\partial t}(\alpha_p \rho_p) + \nabla \cdot (\alpha_p \rho_p \vec{V}_p) = \sum_{q=1}^{nphases} (\dot{m}_{fp} - \dot{m}_{pf}) \tag{1}$$

where subscripts p and f refer to the solid and fluid phase, respecively α_p is the volume fraction, ρ_p is the density of the individual phase, $\vec{V}_p$ is the velocity of the p phase and $\dot{m}_{pf}$ is the mass transfer from the p^{th} to f^{th} phase, respectively. Similarly, the momentum conservation equation for the solid phase is given by:

$$\begin{aligned} \frac{\partial}{\partial t}(\alpha_p \rho_p \vec{V}_p) + \nabla \cdot (\alpha_p \rho_p \vec{V}_p \vec{V}_p) \\ = -\alpha_p \nabla_p + \nabla \cdot \left[\alpha_p \mu_p \left(\nabla_{\vec{V}_p} + \nabla_{\vec{V}_p^T}\right)\right] + \alpha_p \rho_p \vec{g} + F_{vm,lift,user} \\ + \sum_{q=1}^{nphases} \left(\vec{K}_{pf}(\vec{V}_p - \vec{V}_f) + \dot{m}_{fp} \vec{V}_{fp} - \dot{m}_{pf} \vec{V}_{pf}\right) \\ + \vec{K}_{DPM}(\vec{V}_{DPM} - \vec{V}_p) + S_{DPM,explicit} \end{aligned} \tag{2}$$

where μ_p is the shear viscosity of the particle phase p, $\vec{K}_{fp}$ is the interphase momentum exchange coefficient between the fluid and particle phases, $F_{vm,lift,user}$ is a lift force (due to velocity gradients in the primary phase flow field), $\vec{V}_p$ and $\vec{V}_f$ are the particle and fluid velocities, respectively. $\vec{V}_{fp}$ is the interphase velocity and is dependent upon the mass transfer $\dot{m}_{fp}$. $S_{DPM,explicit}$ is the explicit component of the particle sink term, and $\vec{V}_{DPM}$ and $\vec{K}_{DPM}$ are the implicit terms of the particle averaged velocity of the considered discrete phase and interphase momentum exchange coefficient, respectively. Note that the equivalent mass/momentum conservation equations for the fluid phase follow the same logic.

The fluid-solid drag function follows the Gidaspow model [36] and is a combination of the Wen and Yu model [37] and the Ergun relation [38]. When the volume fraction, α_p is greater than 0.8 then the Wen-Yu equation is used, whereas when the volume fraction is less than 0.8 the Ergun relation is used [39]. Relevant modifications have been made by ANSYS for the Ergun relation (Eq.4). The fluid-solid exchange coefficient is given by:

α_p>0.8

$$K_{sl} = \frac{3}{4} C_D \frac{\alpha_S \alpha_f \rho_f |\vec{v}_f - \vec{v}_p|}{d_p} \alpha_l^{-2.65} \tag{3}$$

α_p<0.8

$$K_{sl} = 150 \frac{(1-\alpha_f)^2 \mu_f}{\alpha_p d_p^2} + 1.75(1-\alpha_f) \frac{\rho_f}{d_p} |\vec{v}_f - \vec{v}_p| \tag{4}$$

where C_D is the drag coefficient, d_p is the diameter of the particles in the solid phase, α_p and α_f are the volume fractions of the solid and fluid phases, respectively, and Re_s is the Reynold's number at the terminal settling condition for a single particle and is expressed as:

$$Re_s = \frac{\rho_f d_p |\vec{v}_p - \vec{v}_f|}{\mu_f} \tag{6}$$

where $\rho_f$and μ_f are the fluid density and the dynamic viscosity, respectively.

The drag coefficient C_D is directly dependent on the Reynolds number and it uses the following criteria:

$$C_D = \begin{cases} 24/Re_s & R_e < 0.55 \\ 24(1.0 + 0.15{Re_s}^{0.687})/Re_s & 0.55 < R_e \leq 1000 \\ 0.44 & R_e > 1000 \end{cases} \quad (7)$$

For the transfer of the DEM particle phase into a DPM injection, Fluent first checks the coordinates of each DEM particle with the fluid cells positions and applies the effects of the particle to the cell that is found to contain it. However, since the particle may overlap more than one fluid cell, a Node Based Averaging (NBA) algorithm is used to smooth the loading, distributing the particle's effects to neighbouring mesh nodes. This reduces grid dependency and computational instability by spreading the particle's effects smoother across the neighbouring cells.

Furthermore, as particles move through the fluid, thermal energy is also exchanged. The temperature change of each particle over time is calculated based on Equation (8). The summation of the convective and conductive heat fluxes [40] is given by:

$$m_P C_P \frac{dT}{dt} = \sum Q_{heat} \quad (8)$$

where m_P, C_P, and T are the mass, specific heat and temperature of the particle material, respectively.

$$\sum Q_{heat} = Q_{PF} + Q_{P1P2} \quad (9)$$

$$Q_{PF} = h_{PF} A_p \Delta T_{PF} \quad (10)$$

$$Q_{P1P2} = h_c \Delta T_{P1P2} \quad (11)$$

$$h_c = \frac{4k_{P1}k_{P2}}{k_{P1} + k_{P2}} \left(\frac{3F_N r^*}{4E^*}\right)^{1/3} \quad (12)$$

$$h_{PF} = \frac{k_F N_u}{d_p} \quad (13)$$

where, h_{PF} is the convective fluid-particle heat transfer coefficient, A_p is the particle surface area, ΔT_{PF} is the temperature difference between the fluid and the particles and Q_{P1P2} is the inter-particle heat flux, respectively. h_c is the conductive heat transfer coefficient between two particles and ΔT_{P1P2} is their temperature difference, k_P is the thermal conductivity of the particles, F_N is their normal force, r^* is the geometric mean of the particles radii and E^* is the effective Young's modulus. The bracketed term of the equation models the contact area between two particles. Finally, K_F is the gas thermal conductivity of the fluid, N_u is the Nusselt number, and d_p is the particle diameter. The presented model does not consider conductive heat transfer from the particles to the geometry.

The Nusselt number has been computed based on the results from Ranz and Marshall (1952) for R_e<200. Detailed information regarding the process can be found in Hobbs (2009). The Nusselt number is given by:

$$N_u = 2 + 0.6{R_e}^{1/2} Pr^{1/3} \qquad R_e < 200 \quad (14)$$

$$Pr = \frac{C\mu}{k} \tag{15}$$

where R_e is the Reynold's number based on the diameter of the individual phase and the relative velocity $|\vec{u}_p - \vec{u}_f|$ and the Pr is the Prandtl number for the subsequent phase.

DEM

In DEM simulations, the main computational challenge is the detection of contacts. To address this EDEM uses an algorithm that utilises a Cartesian grid to search for particle contacts. In particular, the domain is divided into grid cells of specified size, then the algorithm checks every cell but only analyses those that contain two or more elements (active cells). The idealized length of a grid cell is 2-6Rmin where R_{min} is the minimum particle radius in the simulation. This reduces the simulation time significantly, while the results remain unaffected by the number of grid cells. Furthermore, the EDEM solver utilises the Hertz–Mindlin contact model [42-44] to solve the contact forces (normal and tangential) between particles, including damping coefficients. For each identified contact the resultant force is calculated taking into consideration the body forces. Particle velocities and new positions, as a result of the forces acting on them, are updated using an explicit time marching scheme. The DEM detection algorithm and calculation cycle are shown in Figure 2(a) and (b), respectively.

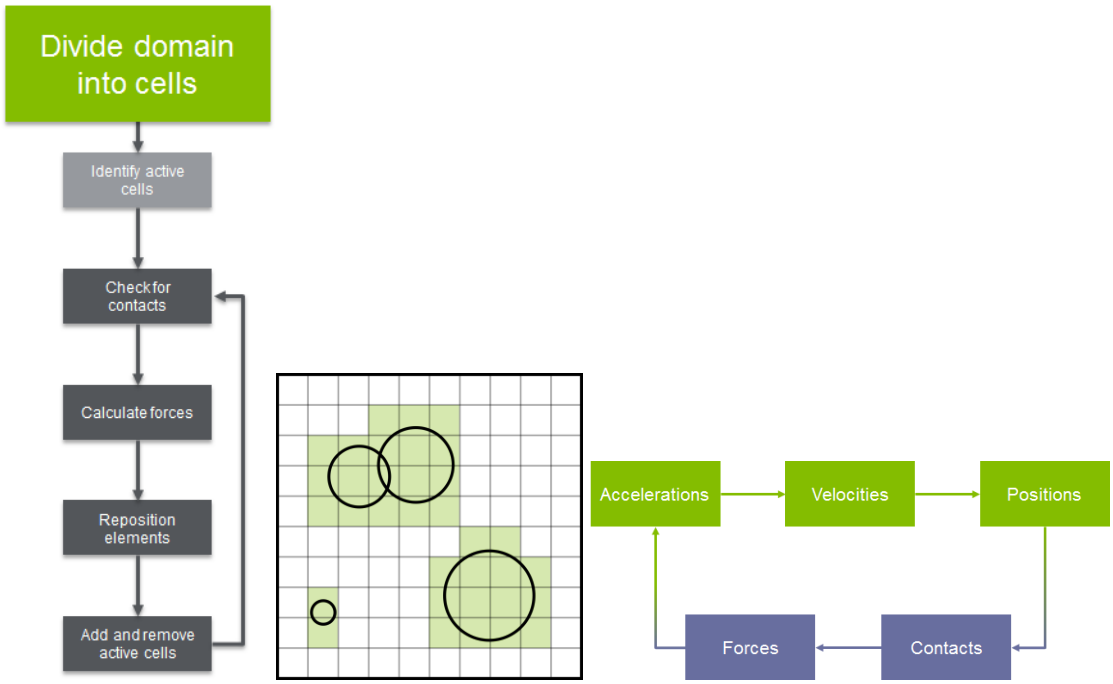

Figure 2 *Schematic of the detection algorithm steps applied on a representative 2D cell grid and the calculation cycle used in the DEM.*

Choosing the right time-step is critical when reducing the simulation time. In EDEM a time-step is chosen as a percentage of the Rayleigh time-step value, which refers to the time taken for a shear wave to propagate through a solid particle, and it is calculated based on the smallest particle of the simulation. The normal range is between 10-40% of the Raleigh time-step and is given by the following equation:

$$T_R = \frac{\pi R \left(\frac{\rho}{G}\right)^{1/2}}{(0.1631v + 0.8766)} \tag{16}$$

where R is the particle radius, ρ the particle density, G the shear modulus and v is the Poisson's ratio.

Figure 3(a) and (b) describe the full coupling methodology and sequence of actions between the two software. EDEM provides a Coupling Interface that includes all the relevant functions that exchange information with Fluent, while Fluent EdemUDF is a user defined function that is loaded into Fluent and handles all drag and heat transfer calculations. Specifically, after setting up the DEM model, EDEM calculates the particles positions and velocities and the DEM-CFD coupling initiates in which the Fluent UDF updates the particle properties taken from EDEM and converts them such that they are passed into Fluent. The latter calculates the volume fraction, drag forces and heat transfer, which are then passed back into EDEM through the UDF and the coupling interface. In general, the DEM time-step tends to be smaller than in CFD and can have a difference between 10 to 1000 times. Therefore, EDEM performs the necessary iterations in order to catch up with the next Fluent time-step and UDF repeats its calculations while passing the data back to Fluent.

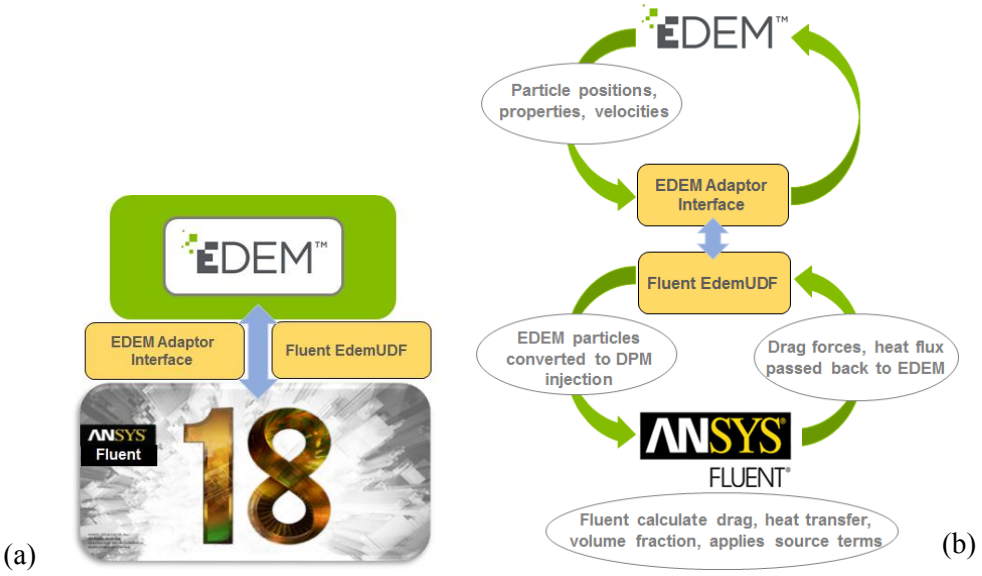

Figure 3 *Schematic of the EDEM-Fluent coupling logic.*

GPU Technology

This project presents an innovative way of accelerating large scale industrial simulations by performing DEM calculations in GPU mode while calculating fluid flow in CPU mode. The EDEM GPU solver provides higher clock speeds compared to simulations on multi-core CPUs.

The presented work has been performed with the use of the EDEM GPU solver engine, created and distributed by DEM Solutions LTD. The EDEM GPU simulation engine uses the Open Computing Language (OpenCL) [45] in combination with the AMD Radeon R9 Fury X graphics card for increased accuracy. OpenCL is an open industry language for general purpose parallel programming across CPUs, GPUs and other processors, that gives complete freedom to users. For example, using OpenCL allows a programmer to write general purpose programs that execute on GPUs without the need to map their algorithms onto a specific vendor's 3D graphics API. Finally, OpenCL creates an efficient programming interface, consisting of an API for coordinating parallel computation across heterogeneous processors, and a cross-platform intermediate language with a well specified computation environment.

Different parallel programming tools exist but the major advantage of using OpenCL is the fact that it fully supports all graphic cards, without tying the DEM user to a single GPU vendor. For example NVIDIA [46] is restricted in using CUDA [47], while OpenCL encapsulates NVIDIA, AMD, Intel Xeon Phi as well as CPUs under a common programming environment. The execution speed and accuracy of arithmetic operations in a computing unit is directly related to the precisión used. Most

computers use the floating-point format, which is an internal representation of numeric values stored in computer memory. This format can be categorized into the single and double precision, where the former requires 4 bytes (32 bits) and the latter 8 bytes (64bits). Even though increasing the number of bits results in increased accuracy, double precision models have much higher memory requirements. Thus, it is critical to select a fitting precision type for a specific application, so that a practical balance between accuracy and simulation time/memory is maintained. The presented results for both graphic cards used single precision.

The presented work uses both the EDEM GPU and CPU solver engines and has been repeated multiple times under different configurations but only selected combinations will be presented herein. The set of simulations, shown in Table 1, used 4CPU cores for the Fluent and 30, 40 CPU cores for EDEM, respectively. Moreover, the same simulation was repeated twice by using the EDEM GPU solver engine with single precision and two different graphics cards; the AMD Radeon R9 Fury X and the NVIDIA Quadro GP100.

Table 1 Configuration combinations for the coupled simulation with the use of the AMD Radeon R9 Fury X and the NVIDIA Quadro GP100 graphic cards.

CPU mode	**GPU mode**	
	AMD Radeon R9 Fury X	**NVIDIA Quadro GP100**
4 Fluent/30 EDEM	4 Fluent/4 EDEM	4 Fluent/4 EDEM
4 Fluent/40 EDEM		

Simulation setup

For this simulation the same geometry and similar setup has been used as presented in Hobbs (2009). Figure 4 demonstrates the 3D model of the aggregate dryer with its internal features (conveying screw flights, veiling flights, combustion flights). A CFD tetrahedral mesh was created by removing all the internal features and preserving mesh density in the burner and combustions zones, whereas a less dense mesh was used in the rest of the geometry.

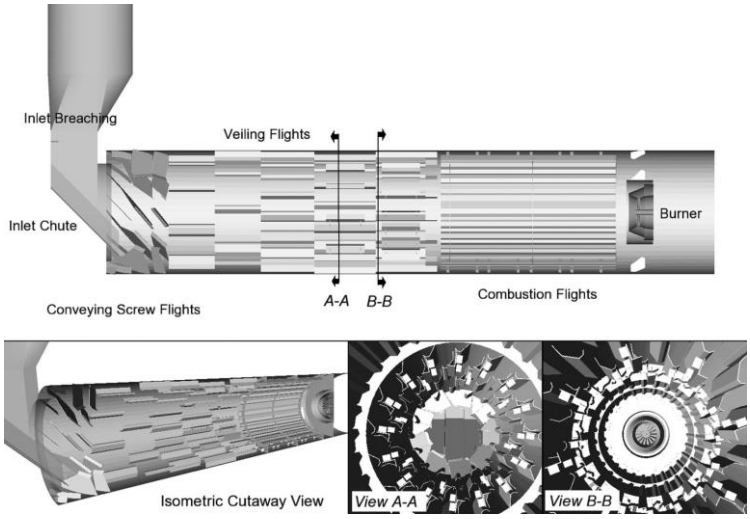

Figure 4 *CAD geometry of the aggregate dryer used for the coupled DEM-CFD simulation [1].*

The full set of the CFD input simulation parameters are shown in Table 2.

Table 2 CFD Input parameters

CFD Input parameters	
Type of fluid	Air
Fluid density (kg/m^3)	1.225
Fluid viscosity (Pa·s)	1.789E-05
Turbulence model	Standard k-ε
CFD cell type	Hybrid tetrahedral hexahedral
Cell number	7.2E+05
CFD time-step (sec)	0.02

The complete 3D drum dryer model was also imported into EDEM. A factory was defined that generated 539.942 discrete elements, comprised of bi-sphered particles of the same size, with a normal distribution and an initial temperature of 300K. The simulated results refer to 1 second of real physical time, after it had reached a quasi-static condition (100sec of run time). A number of trials were performed to determine the optimum time-step and simulating parameters, such as the cell size of the simulator grid. The full set of EDEM inputs are shown in Table 3.

Table 3 EDEM Input parameters

EDEM Input parameters	
Physics	Hertz-Mindlin contact model
Particle density (kg/m^3)	2900
Particle diameter (mm)	18
Particle Shear modulus (Pa)	1.38E+07
Particle Poisson's ratio	0.25
Geometry density (kg/m^3)	7800
Geometry Shear modulus (Pa)	7.50e+07
Geometry Poisson's ratio	0.30
Particle-Particle coefficient of restitution	0.45
Particle-Particle static friction coefficient	0.55
Particle-Particle rolling friction coefficient	0.05
Particle-Geometry coefficient of restitution	0.50
Particle-Geometry static friction coefficient	0.45
Particle-Geometry rolling coefficient	0.05
Particle generation rate (kg/sec)	80.64
EDEM time-step (sec)	1E-04
Cell size (mm)	31.49

Results and discussion

To post-process the CFD-DEM results, Ensight from CEI and EDEM Analyst were used. Figure 5 shows a side view of the aggregate dryer that demonstrates the swirling flow and the fluid-particle temperature distributions ranking 300-3000K and 300-1000K, respectively. The figure also includes

cross sections of the drum at specified points (A,B,C) showing the convective heat transfer. It can be observed that the neighbouring to the burner particles have higher temperatures and the fluid temperature is almost a 3-step decrease of flow. This indicates that as the particles are showered through the hot gases, thermal energy is exchanged and the heat is transferred from the fluid to the particles thus the fluid temperature drops. This particle-fluid behaviour is in very good agreement with the actual observations, validating the model.

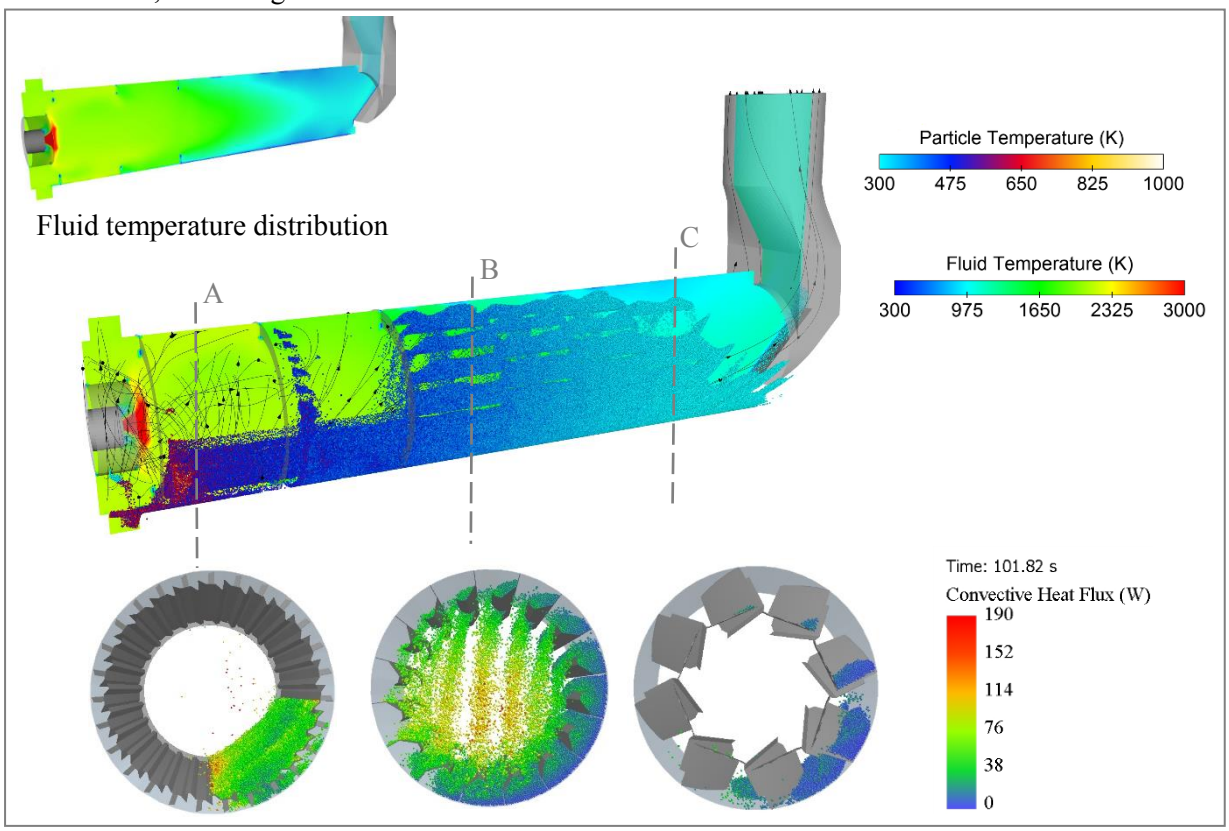

Figure 5 *Coupled CFD-DEM simulation of an aggregate dryer demonstrating the fluid - particle temperature distribution.*

Figure 6 demonstrates an inside view of the heat transfer from the fluid phase to the particle phase. It can be observed that the convective heat flux reaches a max value of around 190W and the simulated model accurately captures the dynamic state of the heat transfer along the length of the drum.

The following figures illustrate the net computational time, under different configurations, for both the EDEM/Fluent coupling and the EDEM part of the simulation. Some representative configurations have been selected for discussion. Figure 7 demonstrates the total computational time of the coupled simulation with and without the GPU solver. Specifically, the selected simulation results in CPU mode (grey columns) used 8, 12 and 32CPU cores for the Fluent part of the simulation and 30 or 40CPU cores for the corresponding EDEM part, respectively. It can be observed that in the first case the simulation took around 1.5 hours, while the simulation times dropped to 1.43 and 1.33 hours, respectively. This shows that even though a large number of cores have been selected, the overall simulation time is only slightly reduced. In contrast, the same simulation run in GPU mode with the use of the AMD Radeon R9 Fury X or the NIVIDIA Quadro GP100 graphic cards leads to reduced simulation times of 1.07 hours and 57minutes, respectively. This means that the NVIDIA Quadro GP100 simulation was 1.5 times faster on average, resulting in an average reduction time of 32%.

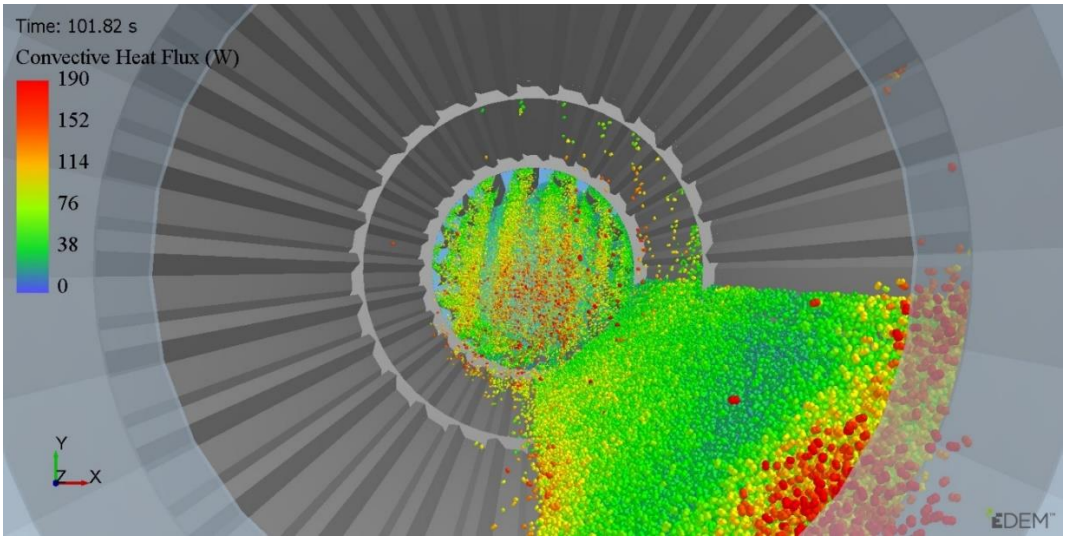

Figure 6 *Particle temperature distribution. Cross sections at the regions close to the burner (A), in the middle of the drum (B), and towards the inlet of the chute (C).*

Figure 8 follows the same logic as Figure 7 demonstrating the net computational time of the aforementioned configurations including only the EDEM part of the simulation. The grey columns show that it took between 39 and 39.25min to simulate the discrete phase for the 30 CPU (for EDEM) configuration and 38.88min for the 40 CPU (for EDEM) configuration. The selected configurations show a minor difference in terms of simulation time, whereas the same simulation took just over 6mins when run in GPU mode (orange column). This corresponds to an average 6.0 speed up demonstrating an average time reduction of 83% for the discrete calculations.

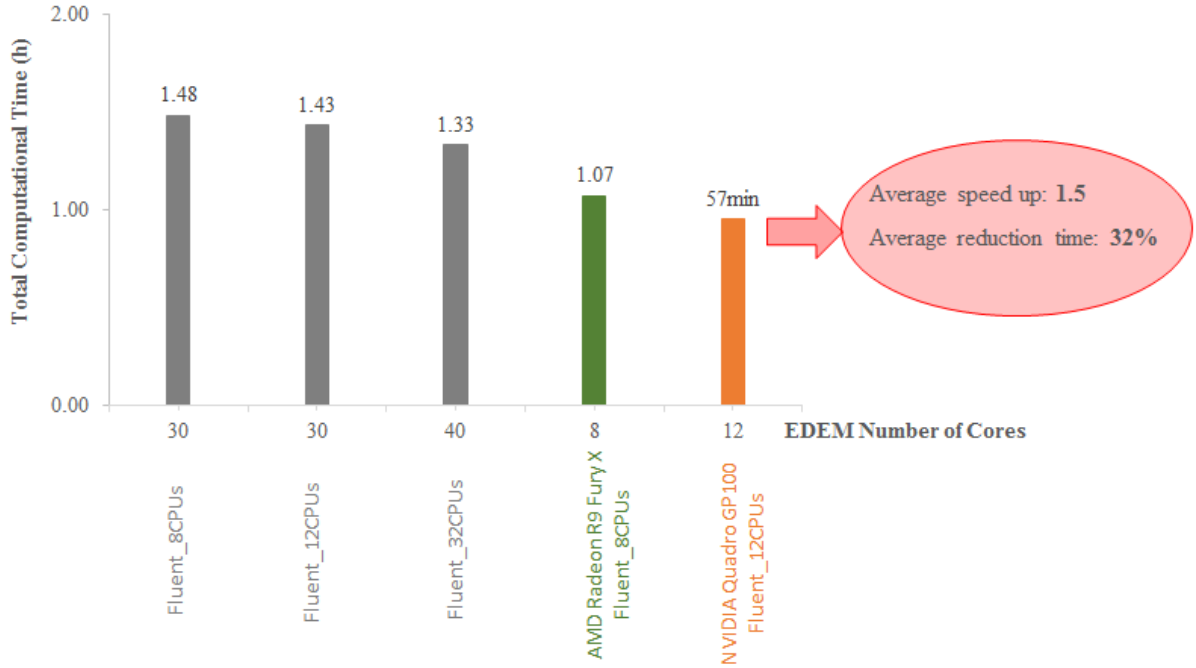

Figure 7 *Net computational time of the coupled simulation under different configurations in CPU mode (grey columns) using the AMD Radeon R9 Fury X graphic card (green), and using the NVIDIA Quadro GP100 (orange).*

Figure 8 *EDEM computational time of the coupled simulation under different configurations in CPU mode (grey columns) using the AMD Radeon R9 Fury X graphic card (green), and using the NVIDIA Quadro GP100 (orange).*

Conclusions

Many industrial applications involve discrete particle flows. Due to their transient nature, they often require extensive computational times and recalculation of the relevant particle physics, which makes such analyses impractical. Until recently the only option to run such simulations was the use of CPU technologies which put a barrier between efficiency and fast results. The current work demonstrates the capabilities and effectiveness of implementing an innovative GPU solver combined with multiple CPU cores to run a complex industrial simulation that models heat transfer within an aggregate drum dryer. The ANSYS Fluent CFD solver has being coupled with EDEM and run with and without the EDEM GPU solver engine.

The results show that the coupled model not only accurately captures the particle-fluid behaviour and the convective heat transfer between the two, but also features very fast simulation run times. With the use of one of the latest GPU graphic cards (NVIDIA Quadro GP100), the net computational time of the coupled DEM-CFD simulation was reduced by 32% corresponding to a 1.5 speed up. Furthermore, the DEM part of the simulation experienced the greatest reduction in computational time with a net computational time reduction of 83%, making the particle calculations 6.0 times faster. More simulations were run with less CPU cores, for both Fluent and EDEM, and the results showed even larger speed ups and time reductions. This indicates that the GPU technology could be very beneficial in cases where less powerful workstations are used for such simulations.

This work highlights the significance of using GPU technology for challenging coupled CFD-DEM calculations. This kind of analysis was previously difficult or even impossible to perform and thus has a major impact in large-scale industrial applications that require simulations of millions of particles.

References

1. Hobbs, A., *Simulation of an aggregate dryer using coupled CFD and DEM methods.* International Journal of Computational Fluid Dynamics, 2009. **23**(2): p. 199-207, http://dx.doi.org/10.1080/10618560802680971.

2. Hockney, R.W., *Computer Simulations Uning Particles*. 2nd ed. 1981, New-York: Routledge.

3. Donzé, F.V., V. Richefeu, and S.-A. Magnier, *Advances in discrete element method applied to soil, rock and concrete mechanics.* Electron J Geotech Eng, 2009. **8**: p. 1-44.

4. Stefanou, I. and I. Vardoulakis. *Stability assessment of SE/E rock corner slope of the Acropolis Hill in Athens*. in *5th GRACM International Congress on Computational Mechanics*. 2005.

5. Date, A.W., *Introduction to computational fluid dynamics*. 2005: Cambridge University Press.

6. Byrne, M.T., et al., *Computational Fluid Dynamics for Reservoir and Well Fluid Flow Performance Modelling*, in *SPE European Formation Damage Conference*. 2011, Society of Petroleum Engineers: Noordwijk, The Netherlands.

7. Wang, S., et al., *Simulation of Flow Behavior of Particles in a Liquid−Solid Fluidized Bed.* Industrial & Engineering Chemistry Research, 2010. **49**(20): p. 10116-10124, http://dx.doi.org/10.1021/ie101139h.

8. Qiu, L.-c. and C.-y. Wu, *A hybrid DEM/CFD approach for solid-liquid flows.* Journal of Hydrodynamics, 2014. **26**(1): p. 19-25, http://www.sciencedirect.com/science/article/pii/S1001605814600032.

9. Fayal, Z.F., B. Lakhdar, and N. Zoubir, *Horizontal Well Performance Flow Simulation CFD-Application*, in *SPE Production and Operations Conference and Exhibition*. 2010, Society of Petroleum Engineers: Tunis, Tunisia.

10. Afsharpoor, A., et al., *CFD modeling of the effect of polymer elasticity on residual oil saturation at the pore-scale.* Journal of Petroleum Science and Engineering, 2012. **94–95**: p. 79-88, http://www.sciencedirect.com/science/article/pii/S0920410512001696.

11. Weinlader, A., et al., *Prediction of the oil flow distribution in oil-immersed transformer windings by network modelling and computational fluid dynamics.* IET Electric Power Applications, 2012. **6**(2): p. 82-90.

12. National Asphalt Pavement Association, N.A.P.A. *History of Asphalt*. 2017. http://www.asphaltpavement.org/index.php?option=com_content&task=view&id=21&Itemid=41.

13. Asphalt Pavement Alliance, A.P.A. *Pavement Technologies*. Pavement Materials, 2017. http://driveasphalt.org/technologies.

14. National Asphalt Pavement Association *Asphalt for Environmental Liners (PS17)*. 1984. http://www.asphaltpavement.org/images/asphalt_environmental1.pdf.

15. Kopal, Z., *Tables of supersonic flow around cones*. 1947, Cambridge: Massachusetts Institute of Technology. 555.

16. Fay, J.A., *Theory of Stagnation Point Heat Transfer in Dissociated Air.* Journal of the Aerospace Sciences, 1958. **25**(2): p. 73-85, http://dx.doi.org/10.2514/8.7517.

17. Blottner, F.G., *Chemical nonequilibrium boundary layer.* AIAA Journal, 1964. **2**(2): p. 232-240, http://dx.doi.org/10.2514/3.2299.

18. Blottner, F.G., *Nonequilibrium laminar boundary-layer flow of ionized air.* AIAA Journal, 1964. **2**(11): p. 1921-1927, http://dx.doi.org/10.2514/3.2701.

19. Hall, H.G., Eschenroeder, A.Q., Marrone, P.V., *Blunt-Nose Inviscid Airflows With Coupled Nonequilibrium Processes.* Journal of the Aerospace Sciences, 1962. **29**(9): p. 1038-1051, http://dx.doi.org/10.2514/8.9690.

20. Biagioli, F., F. Guethe, and B. Schuermans, *Combustion dynamics linked to flame behaviour in a partially premixed swirled industrial burner.* Experimental Thermal and Fluid Science, 2008: p. Medium: X; Size: page(s) 1344-1353.

21. Dupont, V., et al., *The reduction of NOx formation in natural gas burner flames.* Fuel, 1993. **72**(4): p. 497-503, http://www.sciencedirect.com/science/article/pii/001623619390108E.

22. Griffiths, W.D. and F. Boysan, *Computational fluid dynamics (CFD) and empirical modelling of the performance of a number of cyclone samplers.* Journal of Aerosol Science, 1996. **27**(2): p. 281-304, http://www.sciencedirect.com/science/article/pii/0021850295005498.

23. Ma, L., D.B. Ingham, and X. Wen, *NUMERICAL MODELLING OF THE FLUID AND PARTICLE PENETRATION THROUGH SMALL SAMPLING CYCLONES.* Journal of Aerosol Science, 2000. **31**(9): p. 1097-1119, http://www.sciencedirect.com/science/article/pii/S0021850200000161.

24. Sousani, M., Ingham, D., Pourkashanian, M., Sheng, Y., Kenneth, I-I. E., *Simulation of the hydraulic fracturing process of fractured rocks by the discrete element method.* Environmental Earth Sciences, 2015. **73**(12): p. 8451-8469, http://dx.doi.org/10.1007/s12665-014-4005-z.

25. Sousani, M., Kenneth, I-I. E., Ingham, D., Pourkashanian, M., Sheng, Y., *Modelling of hydraulic fracturing process by coupled discrete element and fluid dynamic methods.* Environmental Earth Sciences, 2014. **72**(9): p. 3383-3399, http://dx.doi.org/10.1007/s12665-014-3244-3.

26. Cundall, P.A. and O.D.L. Strack, *A discrete numerical model for granular assemblies.* Géotechnique, 1979. **29**(1): p. 47-65, http://www.icevirtuallibrary.com/doi/abs/10.1680/geot.1979.29.1.47.

27. Kim, B.S., S.W. Park, and S. Kato, *DEM simulation of collapse behaviours of unsaturated granular materials under general stress states.* Computers and Geotechnics, 2012. **42**: p. 52-61, http://www.sciencedirect.com/science/article/pii/S0266352X11002047.

28. McKinnon, S.D. and I. Garrido de la Barra, *Stress field analysis at the El Teniente Mine: evidence for N–S compression in the modern Andes.* Journal of Structural Geology, 2003. **25**(12): p. 2125-2139, http://www.sciencedirect.com/science/article/pii/S0191814103000683.

29. Baird, A.F. and S.D. McKinnon, *Linking stress field deflection to basement structures in southern Ontario: Results from numerical modelling.* Tectonophysics, 2007. **432**(1–4): p. 89-100, http://www.sciencedirect.com/science/article/pii/S0040195106005476.

30. Pantaleev, S., et al., *An experimentally validated DEM study of powder mixing in a paddle blade mixer.* Powder Technology, 2017. **311**: p. 287-302, http://www.sciencedirect.com/science/article/pii/S0032591016309305.

31. Romuli, S., S. Karaj, and J. Müller, *Discrete element method simulation of the hulling process of Jatropha curcas L. fruits.* Biosystems Engineering, 2017. **155**: p. 55-67, http://www.sciencedirect.com/science/article/pii/S1537511016305499.

32. Johansson, M., et al., *Cone crusher performance evaluation using DEM simulations and laboratory experiments for model validation.* Minerals Engineering, 2017. **103–104**: p. 93-101, http://www.sciencedirect.com/science/article/pii/S0892687516303235.

33. Tsuji, Y., Kawaguchi, T.,Tanaka, T., *Discrete particle simulation of two-dimensional fluidized bed.* Powder Technology, 1993. **77**(1): p. 79-87, http://www.sciencedirect.com/science/article/pii/0032591093850107.

34. Tsuji, T., Yabumoto, K., Tanaka, T., *Spontaneous structures in three-dimensional bubbling gas-fluidized bed by parallel DEM–CFD coupling simulation.* Powder Technology, 2008. **184**(2): p. 132-140, http://www.sciencedirect.com/science/article/pii/S003259100700592X.

35. Xu, B.H. and A.B. Yu, *Numerical simulation of the gas-solid flow in a fluidized bed by combining discrete particle method with computational fluid dynamics.* Chemical Engineering Science, 1997. **52**(16): p. 2785-2809, http://www.sciencedirect.com/science/article/pii/S000925099700081X.

36. Gidaspow, D., Bezburuah, R., Ding, J., *Hydrodynamics of circulating fluidized beds: Kinetic theory approach*. Conference: 7th international conference on fluidization. 1991, Chicago, US: Illinois Instute of Techonology. 8.

37. Wen, C.Y., Yu, Y. H., *Mechanics of Fluidization.* The Chemical Engineering Progress Symposium Series, 1966. **62**(62): p. 100-111.

38. Ergun, S., *Fluid flow through packed columns.* Chemical Engineering Progress, 1952. **48**(2): p. 89-94, http://ci.nii.ac.jp/naid/10003393451/.

39. Benzarti, S., H. Mhiri, and H. Bournot, *Drag models for simulation gas-solid flow in the bubbling fluidized bed of FCC particles.* World Academy of Science, Engineering and Technology, 2012. **61**: p. 1138-1143.

40. Chaudhuri, B., F.J. Muzzio, and M.S. Tomassone, *Modeling of heat transfer in granular flow in rotating vessels.* Chemical Engineering Science, 2006. **61**(19): p. 6348-6360, http://www.sciencedirect.com/science/article/pii/S0009250906003393.

41. Ranz, W.E. and W.R. Marshall, *Evaporation from drops.* Chemical Engineering Progress, 1952. **48**(3): p. 141-146.

42. Hertz, H., *On the Contact of Rigid Elastic Solids and on Hardness.* Ch 6: Assorted Papers, 1882.

43. Mindlin, R.D., *Compliance of elastic bodies in contact.* J. Appl. Mech., 1949. **16**: p. 259-268.

44. Deresiewicz, H., Mindlin, R. D., *Elastic spheres in contact under varying oblique forces*. 1952, Columbia University, US: Department of Civil Engineering.

45. Khronos OpenCL Working Group, *The OpenCL Specification*, L. Howes, Editor. 2015.

46. nVIDIA. *NVIDIA'S INVENTION OF THE GPU*. [cited 2017 03 April]; Available from: http://www.nvidia.co.uk/object/about-nvidia-uk.html.

47. nVIDIA. *What is CUDA*. [cited 2017 03 April]; Available from: http://www.nvidia.com/object/cuda_home_new.html.